Can the 62 day X-ray period of ULX M82 X-1 be due to a precessing accretion disk?

Dheeraj R. Pasham[1] & Tod E. Strohmayer[2]

ABSTRACT

We have analyzed all the archival *RXTE/PCA* monitoring observations of the ultraluminous X-ray source (ULX) M82 X-1 in order to study the properties of its previously discovered 62 day X-ray period (Kaaret & Feng 2007). Based on the high coherence of the modulation it has been argued that the observed period is the orbital period of the binary. Utilizing a much longer data set than in previous studies we find: (1) The phase-resolved X-ray (3-15 keV) energy spectra – modeled with a thermal accretion disk and a power-law corona – suggest that the accretion disk's contribution to the total flux is responsible for the overall periodic modulation while the power-law flux remains approximately constant with phase. (2) Suggestive evidence for a sudden phase shift–of approximately 0.3 in phase (20 days)–between the first and the second halves of the light curve separated by roughly 1000 days. If confirmed, the implied timescale to change the period is $\approx$ 10 yrs, which is exceptionally fast for an orbital phenomenon. These independent pieces of evidence are consistent with the 62 day period being due to a precessing accretion disk, similar to the so-called super-orbital periods observed in systems like Her X-1, LMC X-4, and SS433. However, the timing evidence for a change in the period needs to be confirmed with additional observations. This should be possible with further monitoring of M82 with instruments such as the X-ray telescope (XRT) on board *Swift*.

Subject headings: X-rays: individual (M82 X-1) — X-rays: binaries — black hole physics — methods: data analysis

1. Introduction

Ultraluminous X-ray sources (ULXs) are bright, point-like X-ray sources in nearby galaxies with apparent luminosities in the range of a few$\times 10^{39-41}$ ergs s^{-1} (Fabbiano 1989;

[1]Astronomy Department, University of Maryland, College Park, MD 20742; dheeraj@astro.umd.edu

[2]Astrophysics Science Division, NASA's Goddard Space Flight Center, Greenbelt, MD 20771; email: tod.strohmayer@nasa.gov

Mushotzky et al. 2004; Swartz et al. 2011). They are mysterious in the sense that their energy output exceeds the theoretical maximum (the Eddington limit: the maximum luminosity beyond which isotropically accreting matter will be driven away by radiation forces) for stellar-mass black holes (mass range of 3-20 $M_{\odot}$) (see reviews by Miller & Colbert 2004 and Feng & Soria 2011). These sources (excluding the X-ray bright supernovae: e.g., Immler & Lewin 2003) could be stellar-mass black holes undergoing super-Eddington accretion and/or emission (King et al. 2001; Begelman 2002; Körding et al. 2002; Gladstone et al. 2009) or the missing class of intermediate-mass black holes (mass range: few$\times$(100-1000) $M_{\odot}$) accreting at sub-Eddington rates (Colbert & Mushotzky 1999; Miller et al. 2004).

With a maximum X-ray luminosity of approximately 10^{41} ergs s^{-1} (Kaaret et al. 2009) M82 X-1 is a remarkably bright ULX. Owing to its high luminosity it is sometimes referred to as a "hyper-luminous X-ray source" (e.g., Matsumoto et al. 2004; Tsuru et al. 2004). Its high average X-ray luminosity of roughly 5×10^{40} ergs s^{-1} combined with the presence of X-ray quasi-periodic oscillations (QPOs) in the frequency range of 0.04-0.2 Hz suggests that it may contain an intermediate-mass black hole of mass roughly 100-1000 $M_{\odot}$ (Strohmayer & Mushotzky 2003; Hopman et al. 2004; Portegies Zwart et al. 2005; Dewangan et al. 2006; Mucciarelli et al. 2006; Pasham & Strohmayer 2013). Another intriguing property – relevant to this work – is that the X-ray intensity of this source varies regularly with a period of 62 days (Kaaret et al. 2006; Kaaret & Feng 2007). Amongst ULXs, such long, periodic X-ray modulations have been seen from two other sources, NGC 5408 X-1 (Strohmayer 2009; Han et al. 2012; Pasham & Strohmayer 2013) and HLX ESO 243-39 (e.g., Servillat et al. 2011). The 62 day period of M82 X-1 has been claimed to be the orbital period of the black hole binary system (Kaaret et al. 2006). Here, we study the properties of this period using new data and present evidence that suggests this modulation may instead be due to the precessing accretion disk of the black hole.

2. Data Primer

All the data used in the present work were obtained with the Rossi X-ray Timing Explorer's (*RXTE*'s) proportional counter array (*PCA*) operating in the *GoodXenon* data acquisition mode. We used data from the monitoring program beginning 2004 September 2 until 2009 December 30 (1945 days), during which M82 was observed roughly once every three days (2-3 ks per observation).

RXTE/PCA is an array of five detectors each referred to as a proportional counter unit (PCU). The individual PCUs are labelled as PCU0-4. PCUs 0, 1, 3 and 4 have been turned on and off irregularly (to avoid damage associated with electrical break-downs) during the

monitoring program. Hence, all the observations of M82 were not carried out with the same set of detectors. However, PCU2 was operating in all the observations, therefore, to be consistent in our analysis we only used data acquired from PCU2. Furthermore, for sources with net count rates less than ≈ 20 counts sec^{-1}, the *RXTE/PCA* data analysis guide provided by *RXTE*'s Guest Observer Facility (http://heasarc.nasa.gov/docs/xte/recipes/layers.html) suggests using only the top Xenon layer to maximize the signal to noise ratio. Therefore, we screened our data to include only events from the top layer (layer-1) with both anode chains (Left and Right). In addition, we imposed the following standard filter on the data: ELV > 10.0 && OFFSET < 0.02 && PCU2_ON == 1 && (TIME_SINCE_SAA < 0 || TIME_SINCE_SAA > 30) && ELECTRON2 < 0.1. Finally, we used the latest SAA history and background model (*pca_bkgd_cmfaintl7_eMv20051128.mdl*) files for our analysis. The screening criteria used here is discussed in detail on NASA/HEASARC's Web page http://heasarc.nasa.gov/docs/xte/abc/screening.html.

The PCA observations were divided amongst six proposals (*RXTE* proposal IDs: P20303, P90121, P90171, P92098, P93123, P94123). We used the *rex* script provided by *RXTE*'s guest observer facility to extract the individual light curves and the energy spectra of the source as well as the background. In addition to the filters described above we only used data from channels 0-35 which translates to X-ray events in the energy range of 3-15 keV.

3. Results

3.1. Timing Analysis

From each of the individual monitoring observations we extracted an average, background subtracted, count rate. This resulted in a total of 810 data points (observations) distributed over a time scale of 1945 days. The complete *RXTE/PCA* 3-15 keV binned light curve of M82 (*solid points*) along with the running-average (*solid curve*) is shown in Figure 1. While the earlier work by Kaaret & Feng (2007) used only the data from day 0 until roughly day 900, i.e., essentially segment 1 of Figure 1, this work includes the entire *RXTE/PCA* monitoring data of M82.

As an initial test for the stability of the period, we over-plotted vertical lines uniformly separated by 62 days[1] and coincident with the expected minima of the light curve assuming this period is constant (dashed vertical lines in Figure 1). It is clear even by eye that while the vertical lines are coincident with the light curve's minima until the large flare occurring

[1]The best-fit period reported by Kaaret & Feng 2007 was 62±0.3 days.

around day 1000, they are offset thereafter. The location of the light curve's minima were estimated as follows. We folded the first four cycles of the data at a period of 62 days, i.e., data from day 0 - day 240. We then fit this folded light curve with a model that includes two Fourier components (the fundamental and the first harmonic), i.e., I = A + Bsin2π(ϕ-ϕ_0) + Csin4π(ϕ-ϕ_1). The folded light curve (*solid points*) along with the best-fit function (*solid curve*) is shown in the left panel of Figure 2. The best-fit model parameters are A = 0.44$\pm$0.01, ϕ_0 = 1.14$\pm$0.01, B = 2.69$\pm$0.02, C = 0.07$\pm$0.01, ϕ_1 = 1.06$\pm$0.01 while the best-fit χ^2 value was 4 for 5 degrees of freedom. If the 62 day modulation were constant throughout the monitoring program then the minima of the best-fit model should track the light curve's minima.

Another way to assess this phase change is to separately fold the segments of the light curve before and after the first large flare (segment 1 and 2 as indicated in Figure 1), at the period of 62 days. Therefore, we divided the complete light curve into two segments: 1) prior to the large flare and 2) after the large flare. For the first segment we used data from day 0 to day 976 where day 976 represents roughly the epoch of the onset of the flare (see Figure 1). For the second segment we used data from day 976 until the end of the light curve. We then transformed the two segments of the light curve to have the same start time. This is essential as a phase difference between the start times of the two segments can manifest as an offset between their folded light curves. After taking care of the start phases, we folded the two segments separately at a period of 62 days[2] as found in the earlier work by Kaaret & Feng (2007). The two folded light curves (offset to have zero mean) are shown in the right panel of Figure 2. Clearly there is a significant phase offset of roughly 0.3 – equivalent to 0.3$\times$62 days $\approx$ 20 days – between the two portions of the light curve.

It is possible that this phase difference is due to an incorrect choice of the fold period. In other words, considering the uncertainty in the period reported by Kaaret & Feng (2007), the actual value of the period can be in the range (90% confidence) 62 ± 0.3 days. Therefore, we repeated the above exercise of comparing the phase lag between the two segments of the light curve using various fold periods between 61.7 and 62.3 days. We find that the lag is significant in all the cases with the lag value varying from roughly 17 to 25 days. However, if we relax the confidence interval on the best-fit period, we find that one can obtain essentially zero lag between the two segments with a fold period of 60.6 days. But we note that this value is 4.7 times the quoted uncertainty, that is, (1.4/0.3) = 4.7, away from the best-fit period of 62 days. Since a 90% confidence region is $\approx 1.6\sigma$ (assuming gaussian statistics) from the best value, then one has to go $1.6 \times 4.7 = 7.5\sigma$ from the best period (62 days) in

[2]Note that we have constructed a Lomb-Scargle periodogram (Scargle 1982; Horne & Baliunas 1986) of segment 2 and find evidence for a power spectral peak that is consistent with a period of 62 days.

order to cancel the inferred lag. This supports the presence of a real phase shift, but due to the relatively modest number of overall cycles present in the data, a confirmation of a varying period would still be important.

4. Energy Spectral Analysis

For the purposes of extracting phase-resolved energy spectra we used only data from day zero until prior to the first large flare around day 1000, i.e., segment 1 of Figure 1. We made this choice for the following reasons: (1) the 62 day modulation is highly coherent during this portion of the data and (2) the greater prevalence of flaring in the second segment likely introduces additional state-related spectral variations which could mask any purely phase-related changes.

We then extracted the energy spectra of the source and the background from each of the individual monitoring observations in segment 1. Using *RXTE/PCA*'s tool *pcarsp* we created responses separately for each of these observations. We then divided these observations into six equal-sized phase bins of size 1/6 using a period of 62 days. Using the FTOOL *sumpha* we combined all the source and the background energy spectra in a given phase bin to obtain six average phase-resolved source and background energy spectra. Similarly using the FTOOLs *addrmf* and *addarf*, we created the six weight-averaged response matrices and the ancillary response functions, respectively. For each of these twelve response files (six RMFs and six ARFs) weights were assigned according to the total number of counts in a given observation. We then binned the energy spectra to ensure a minimum of 30 counts in each spectral bin.

We then modeled each of these six energy spectra with a blackbody disk, a power-law model, and a gaussian component to account for the weakly broadened Fe Kα emission line. We used the *XSPEC* (Arnaud 1996) spectral fitting package to fit all our spectra. In terms of *XSPEC* models, we used *phabs*(diskpn + gauss + pow)*. The spectral resolution of the data does not allow us to constrain the Gaussian parameters but it is required for a good fit. Therefore, we fixed the centroid energy and the width of the iron line at 6.55 keV and 0.33 keV, respectively. We obtained these values from earlier work using high-resolution *Suzaku* and *XMM-Newton* observations of M82 X-1 (Strohmayer & Mushotzky 2003; Caballero-García 2011). Furthermore, the quality of the data does not allow us to independently constrain each of the model's parameters. To break the degeneracy either the disk temperature or the index of the power-law component had to be frozen. We obtained the best-fitting parameters in both these cases. We find that in the energy range of 3-15 keV this model fits the data well giving reduced χ^2 values in the range of 0.6-1.1 for 24 degrees of freedom. All the best-fit model parameters are indicated in Table 1. While the left-hand

side of Figure 4 shows the value of the disk and the power-law fluxes as a function of the phase with the power-law index fixed, the right-hand side shows the dependence of these fluxes on the phase for the case where disk temperature was fixed. Clearly, the disk flux varies with phase in both cases while the power-law flux remains essentially constant.

5. Discussion

The phase offset noted above (≈ 0.3 cycles or about 20 days) occurs over a timescale of roughly 1000 days, the time interval between segment 1 and 2 of Figure 1. This corresponds to a characteristic timescale of $1/(0.3/1000)$ or $\sim$ 10 yrs. This is unusually fast for an orbital phenomenon. The typical values of evolution timescales of orbits of accreting compact binaries (neutron star or black hole binaries) is a few$\times 10^6$ yrs (e.g., Verbunt 1993; Levine et al. 2000; Baykal et al. 2006; Wolff et al. 2009; Jain et al. 2010 and references therein). This suggests that the evolutionary timescale of the phenomenon associated with the 62 day period may be $\sim 10^5$ times faster than any known accreting compact binary's orbital period. Periods longer than the orbital period have been detected from numerous compact binaries (e.g., Kotze & Charles 2012, KC12 hereafter; Wen et al. 2006, W06 hereafter). These are known as super-orbital periods and are ascribed to the precessing accretion disks of the respective compact sources (e.g., Katz 1973; Pringle 1996; Ogilvie & Dubus 2001). A characterstic feature of super-orbital periods is that they are often accompanied by sudden changes in coherence, either in the period or the phase, similar to the suggested behavior reported here from M82.

On the other hand, there are numerous systems which exhibit relatively stable super-orbital periods. These include Her X-1 with a period between 33-37 days (e.g., Leahy & Igna 2010; Also see Figure 16 of KC12), LMC X-4 with $\sim$ 30 days (W06; See Figure 5 of KC12), and SS433 with a period of $\sim$ 162 days (W06; See Figure 7 of KC12). 2S 0114+650 also shows a stable super-orbital period (see Figure 8 of KC12) but this may not be due to a precessing accretion disk (e.g., Farrell et al. 2006). At least in Her X-1 phase shifts are known to occur (see, for example, Figure 9 of Clarkson et al. 2003) just before the onset of the so-called anomalous low state. It is perhaps an interesting coincidence that the phase shift in M82 occurs just prior to the flare (see Figure 1). It is also known that M82 X-1 – presumably the source of the 62 day modulation – underwent a transition into the thermal dominant state during the flare (Feng & Kaaret 2010). Thus it remains speculative that the flare may have been associated with the phase offset.

Moreover, if this modulation is indeed due to a precessing accretion disk one expects the X-ray flux originating from the disk to vary periodically with a period of 62 days. This

is simply due to the fact that as the accretion disk precesses, the effective sky projected area of the disk – and hence the disk flux whose value is proportional to the area of the emitting surface, i.e., the projected disk area – varies with the phase of the precession period. The observed dependence of the disk flux with the phase of the 62 day period is consistent with this idea (see Figure 4).

One of the biggest controversies surrounding M82 X-1 is whether it hosts an intermediate-mass or a stellar-mass black hole. If the 62 day period is indeed due to relatively stable precession of the accretion disk – presumably due to radiation induced warping – then probing the warp structure can, in principle, give us some insight into the mass question. Given the accretion efficiency of the black hole (ϵ) and the ratio of the viscosity in the normal to the planar direction (η), Pringle (1996) derived the radius beyond which the disk warps. This radius (R) is as follows:

$$\frac{R}{R_s} \geq \left(\frac{2\sqrt{2}\pi\eta}{\epsilon}\right)^2 \tag{1}$$

where R_s is the Schwarzschild radius ($2GM/c^2$). The value of η is ~ 1 (Pringle 1996). As noted earlier, M82 X-1 has an average luminosity of $5{\times}10^{40}$ ergs s^{-1}. Assuming isotropic emission the relation connecting the mass of the black hole (M), the accretion efficiency (ϵ) and the luminosity (L) is given by:

$$L = 1.38 \times 10^{38} \times \frac{\epsilon M}{M_\odot}\ ergs\ s^{-1} \tag{2}$$

where M has the units of $M_\odot$. Now, if M82 X-1 were hosting an intermediate mass black hole of mass, say, a few 1000 M$_\odot$, the value of ϵ is of the order of 0.1. The radii at which the disk warps is then $\sim$ a few 1000 R$_s$. On the other hand, if the source were a stellar-mass black hole, say of 20 M$_\odot$, the value of ϵ is of the order of 10 which results in warping at radii of a few R$_s$, i.e., the innermost regions of the disk.

The majority of the disk flux is emitted from the innermost regions of the accretion disk ($\sim$ a few 10 R$_s$), by the gravitational energy loss of the in-falling material. As noted above – based on the mass of the black hole within M82 X-1 – there are two possible disk structures: (1) where the inner disk is warped while the outer disk remains flat (stellar-mass black hole scenario) or (2) the outer disk is warped with the inner disk remaining flat (intermediate-mass black hole scenario). In the first case, as the innermost disk precesses the X-ray disk flux originating from this region will also modulate at the precession period thus naturally explaining the disk modulation observed here (Figure 4). In the second case

the direct disk emission is expected to remain constant with the precession period. However, the disk photons can reflect off the warp in the outer disk and this reflected component will modulate at the precession period. In this case the reflection can also produce emission features, viz., Fe kα. The strength of the reflection is proportional to the projected surface area of the warped disk where reflection occurs. Therefore any such emission lines would be expected to vary periodically with the phase of the precession period. The quality of the current data (Table 1) does not allow us to solve this problem, however, this should be possible in the near future using phase-resolved X-ray spectroscopy.

6. Orbital Scenario and caveats

While our results show that the 62 day period of M82 X-1 may be due to a precessing accretion disk they do not yet rule out the possibility that it might be orbital in nature. In the standard picture of periodic X-ray modulations from X-ray binaries obscuration by, for example, a hot spot at the edge of the accretion disk (accretion stream interaction site: see Parmar & White 1988; Armitage & Livio 1998) is thought to be the source of the regular variations with periods equal to the orbital period of the system. It is interesting to note that in the present case, the phase offset appears to occur just prior to the large flare occurring around day 1000. Assuming that the standard hot spot model is at play here, it is conceivable that a sudden influx in the accreting material may have shifted the hot spot and caused an apparent phase shift. Furthermore, the flux from M82 (Figure 1) is a combination of multiple sources with *RXTE*'s field-of-view (Matsumoto et al. 2001). It is possible that the constant power-law component (bottom panels of Figure 4) is due to the combined contribution from the contaminating sources while the majority of the disk component originates from M82 X-1. If this were the case, one naturally expects the modulation profile seen in Figure 4. Moreover, the assumption of a thermal accretion disk and a power-law corona for the X-ray energy spectra of ULXs has been questioned (see. e.g., Gladstone et al. 2009).

In summary, our results suggest that the 62 day X-ray period of M82 X-1 may be due to a precessing accretion disk. This hypothesis would be greatly strengthened if a variation in the observed periodicity can be confirmed. This can be explored with future monitoring observations using instruments such as the X-ray telescope on board *Swift*.

We thank Dr. Richard Mushotzky, Dr. Margaret Trippe, Dr. Coleman Miller, Dr. Phil Kaaret, Dr. Robert Olling and Dr. Chris Reynolds for valuable suggestions and critical comments.

REFERENCES

Armitage, P. J., & Livio, M. 1998, ApJ, 493, 898

Arnaud, K. A. 1996, Astronomical Data Analysis Software and Systems V, 101, 17

Baykal, A., Inam, S. Ç., & Beklen, E. 2006, A&A, 453, 1037

Begelman, M. C. 2002, ApJ, 568, L97

Caballero-García, M. D. 2011, MNRAS, 418, 1973

Clarkson, W. I., Charles, P. A., Coe, M. J., & Laycock, S. 2003, MNRAS, 343, 1213

Colbert, E. J. M., & Mushotzky, R. F. 1999, ApJ, 519, 89

Dewangan, G. C., Titarchuk, L., & Griffiths, R. E. 2006, ApJ, 637, L21

Fabbiano, G. 1989, ARA&A, 27, 87

Farrell, S. A., Sood, R. K., & O'Neill, P. M. 2006, MNRAS, 367, 1457

Feng, H., & Kaaret, P. 2010, ApJ, 712, L169

Feng, H., & Soria, R. 2011, New A Rev., 55, 166

Gladstone, J. C., Roberts, T. P., & Done, C. 2009, MNRAS, 397, 1836

Han, X., An, T., Wang, J.-Y., et al. 2012, Research in Astronomy and Astrophysics, 12, 1597

Hopman, C., Portegies Zwart, S. F., & Alexander, T. 2004, ApJ, 604, L101

Horne, J. H., & Baliunas, S. L. 1986, ApJ, 302, 757

Immler, S., & Lewin, W. H. G. 2003, Supernovae and Gamma-Ray Bursters, 598, 91

Jain, C., Paul, B., & Dutta, A. 2010, MNRAS, 409, 755

Kaaret, P., Simet, M. G., & Lang, C. C. 2006, ApJ, 646, 174

Kaaret, P., & Feng, H. 2007, ApJ, 669, 106

Kaaret, P., Feng, H., & Gorski, M. 2009, ApJ, 692, 653

Katz, J. I. 1973, Nature Physical Science, 246, 87

King, A. R., Davies, M. B., Ward, M. J., Fabbiano, G., & Elvis, M. 2001, ApJ, 552, L109

Körding, E., Falcke, H., & Markoff, S. 2002, A&A, 382, L13

Kotze, M. M., & Charles, P. A. 2012, MNRAS, 420, 1575

Leahy, D. A., & Igna, C. D. 2010, ApJ, 713, 318

Levine, A. M., Rappaport, S. A., & Zojcheski, G. 2000, ApJ, 541, 194

Matsumoto, H., Tsuru, T. G., Koyama, K., et al. 2001, ApJ, 547, L25

Matsumoto, H., Tatsuya, I., Tsuru, T. G., et al. 2004, Progress of Theoretical Physics Supplement, 155, 379

Miller, M. C., & Colbert, E. J. M. 2004, International Journal of Modern Physics D, 13, 1

Miller, J. M., Fabian,A. C., & Miller, M. C. 2004, ApJ, 614, L117

Mucciarelli, P., Casella, P., Belloni, T., Zampieri, L., & Ranalli, P. 2006, MNRAS, 365, 1123

Mushotzky, R. 2004, Progress of Theoretical Physics Supplement, 155, 27

Ogilvie, G. I., & Dubus, G. 2001, MNRAS, 320, 485

Parmar, A. N., & White, N. E. 1988, Mem. Soc. Astron. Italiana, 59, 147

Pasham, D. R., & Strohmayer, T. E. 2013, ApJ, 764, 93

Pasham, D. R., & Strohmayer, T. E. 2013, ApJ, 771, 1

Portegies Zwart, S. F., Dewi, J., & Maccarone, T. 2005, Ap&SS, 300, 247

Pringle, J. E. 1996, MNRAS, 281, 357

Scargle, J. D. 1982, ApJ, 263, 835

Servillat, M., Farrell, S. A., Lin, D., et al. 2011, ApJ, 743, 6

Strohmayer, T. E., & Mushotzky, R. F. 2003, ApJ, 586, L61

Strohmayer, T. E. 2009, ApJ, 706, L210

Swartz, D. A., Soria, R., Tennant, A. F., & Yukita, M. 2011, ApJ, 741, 49

Tsuru, T. G., Matsumoto, H., Inui, T., et al. 2004, Progress of Theoretical Physics Supplement, 155, 59

Verbunt, F. 1993, ARA&A, 31, 93

Wen, L., Levine, A. M., Corbet, R. H. D., & Bradt, H. V. 2006, ApJS, 163, 372

Wolff, M. T., Ray, P. S., Wood, K. S., & Hertz, P. L. 2009, ApJS, 183, 156

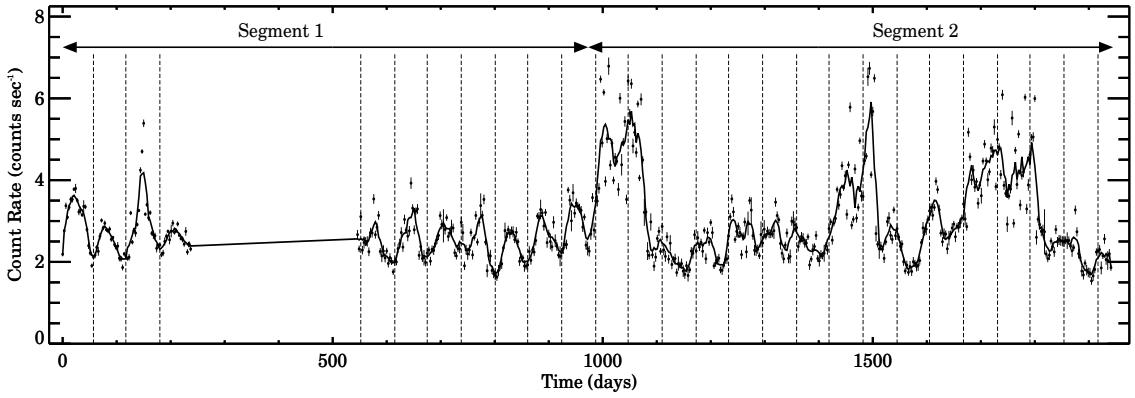

Figure 1. Complete RXTE/PCA binned X-ray (3-15 keV) light curve of M82 (*solid points*) along with the running average (*solid curve*) that traces the overall X-ray variability of M82. The error bars on the individual data points are also shown. The start time of the light curve is 2004 September 2, 14:26:14.757 UTC. The bin size is 3 days. We chose this particular bin size as the time interval between consecutive observations was less than 3 days during $> 95\%$ of the monitoring program. In the rest 5% of the data we extrapolated linearly. The running average was obtained by averaging over five bins around a given bin. The gap in the data from roughly day 240 to day 550 is because the source was not observed by RXTE during this time. This solid curve traces the overall X-ray variability of M82 X-1. The vertical lines show the expected minima of the X-ray modulation assuming the 62 day period remains constant all throughout the data. The two segments represent data before and after the first major flare that occurs around day 1000. It is obvious that the locations of the minima, as indicated by the vertical lines, do not match the light curve's minima during segment 2.

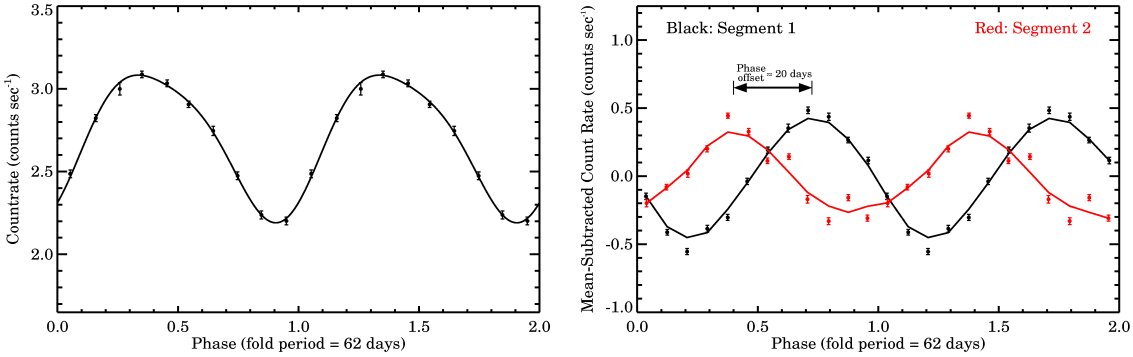

Figure 2. Left Panel: Folded X-ray (3-15 keV) light curve of M82 (*solid points*) along with the best-fit sinusoid curve (*solid curve*) using only data from day 0 until day 240 (see text). 10 bins per cycle were used and two cycles are shown to guide the eye. Right Panel: Mean-subtracted folded X-ray (3-15 keV) light curves of M82 during segment 1 (black) and 2 (red). In each case a total of 12 bins per cycle were used and two cycles are shown for clarity. The error bars on the individual phase bins are also shown. The solid curves represent the running average over three neighboring bins. A phase offset of $\approx$ 20 days between the two portions of the light curve is evident. Due to episodes of high count rate (for example the flare around day 1000) the average count rate during segment 2 is higher compared to the average value during segment 1. In order to clearly show the phase offset, we have subtracted the mean count rate from each folded light curve.

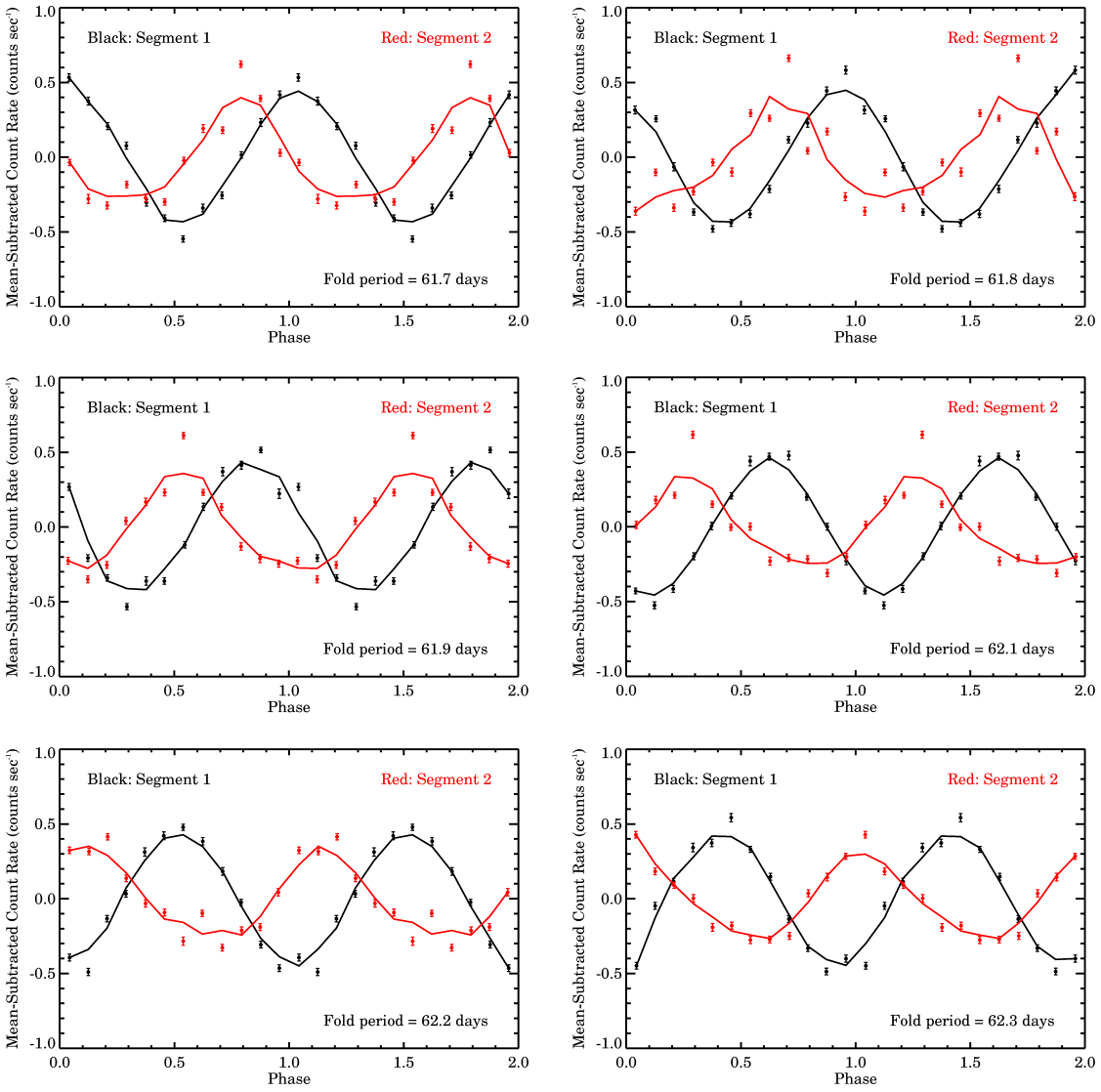

Figure 3. Mean-subtracted folded X-ray (3-15 keV) light curves of M82 during segment 1 (black) and 2 (red) of the light curve using various fold periods within the error bar reported by Kaaret & Feng (2007). Similar to the right panel of Figure 2, in each case 12 bins per cycle are used and two cycles are shown for clarity. The solid curves represent the running mean taken over three meighboring bins in each case. The fold period used for the top left, top right, middle left, middle right, bottom left, bottom right are 61.7, 61.8, 61.9, 62.1, 62.2, 62.3 days, respectively. A significant "phase-offset" is evident in each case.

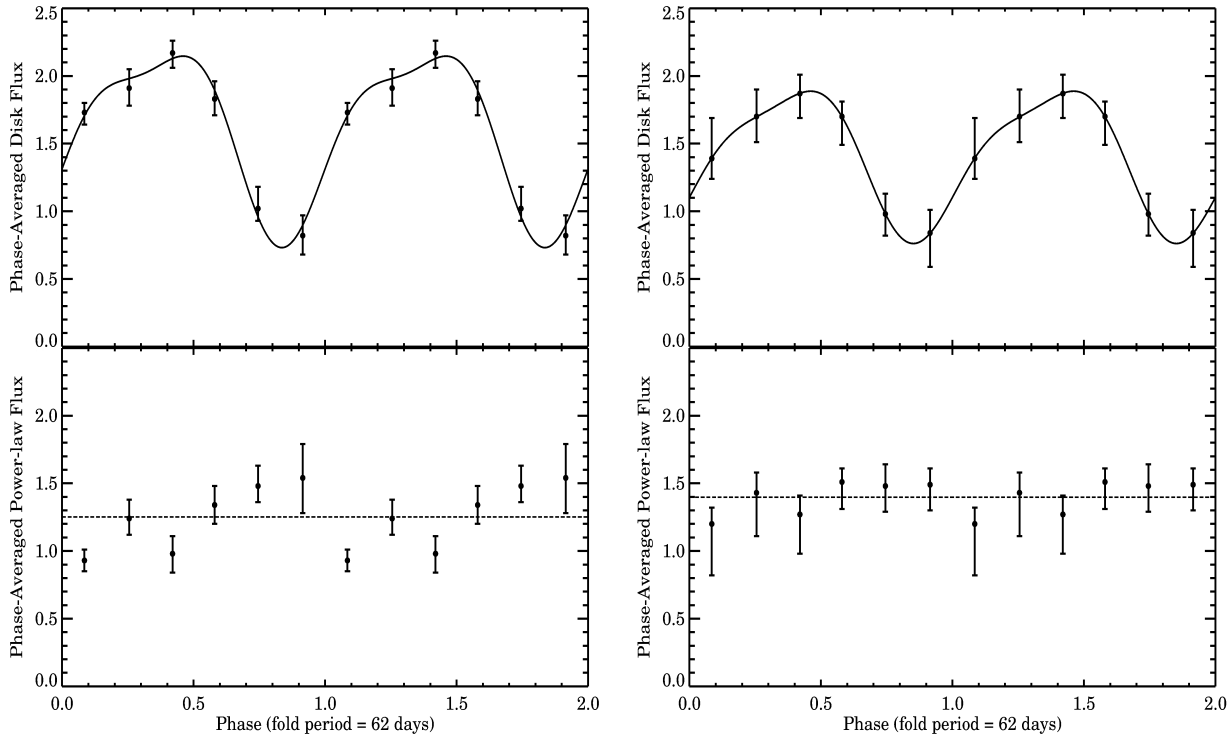

Figure 4. Left panels: The phase-average X-ray (3-15 keV) disk flux (*y-axis* in the top left panel) and the power-law flux (*y-axis* in the bottom left panel) as a function of the 62 day phase (*x-axis*) when the power-law index was fixed. Right panels: Same as the left panels but disk temperature was fixed instead. The flux units are 10^{-11} ergs s^{-1} cm^{-2}. In each case two cycles are shown for clarity. In order to guide the eye, the best-fitting sinusoid curves (*solid*) defined as A + B*Sin[2π(phase-constant$_0$)] + C*Sin[4π(phase-constant$_1$)] are also indicated in the two top panels. The horizontal lines in the bottom panels indicate the average power-law fluxes in the two cases. All the error bars above represent 1σ uncertainty on the flux. Clearly, the X-ray modulation is essentially due to the disk component.

Table 1: Summary of the phase-averaged energy spectral modeling of M82 X-1. Best-fitting parameters using the *phabs∗(diskpn+gauss+pow)* model are shown.

phabs∗(diskpn+gauss+pow):						
Fixed power-law index						
Phase[a]	0.085	0.255	0.420	0.58	0.745	0.915
T^{b}_{max}	$1.9^{+0.1}_{-0.1}$	$2.0^{+0.1}_{-0.1}$	$2.0^{+0.1}_{-0.1}$	$2.1^{+0.1}_{-0.1}$	$2.1^{+0.1}_{-0.1}$	$2.4^{+0.2}_{-0.2}$
N^{c}_{disk}	$14.4^{+2.6}_{-2.1}$	$13.8^{+2.3}_{-1.9}$	$15.8^{+2.6}_{-2.2}$	$9.7^{+1.2}_{-1.0}$	$5.6^{+0.8}_{-0.7}$	$2.7^{+1.0}_{-0.9}$
N^{d}_{gauss}	$4.1^{+1.2}_{-1.2}$	$4.3^{+1.3}_{-1.3}$	$3.6^{+1.4}_{-1.4}$	$3.5^{+1.2}_{-1.2}$	$4.3^{+1.2}_{-1.2}$	$4.6^{+1.4}_{-1.4}$
Γ^{e}	1.1	1.4	1.1	1.6	1.9	2.1
N^{e}_{powlaw}	$0.62^{+0.1}_{-0.1}$	$1.33^{+0.2}_{-0.2}$	$0.58^{+0.1}_{-0.1}$	$2.5^{+0.4}_{-0.4}$	$4.8^{+0.8}_{-0.8}$	$7.6^{+1.5}_{-1.5}$
F^{f}_{X}	$2.71^{+0.02}_{-0.02}$	$3.21^{+0.02}_{-0.02}$	$3.21^{+0.03}_{-0.03}$	$3.20^{+0.03}_{-0.02}$	$2.55^{+0.03}_{-0.03}$	$2.35^{+0.03}_{-0.04}$
F^{f}_{Disk}	$1.73^{+0.07}_{-0.09}$	$1.91^{+0.14}_{-0.13}$	$2.17^{+0.09}_{-0.11}$	$1.83^{+0.13}_{-0.12}$	$1.02^{+0.16}_{-0.09}$	$0.82^{+0.15}_{-0.14}$
F^{f}_{Power}	$0.93^{+0.08}_{-0.08}$	$1.24^{+0.14}_{-0.12}$	$0.98^{+0.13}_{-0.14}$	$1.34^{+0.14}_{-0.14}$	$1.48^{+0.15}_{-0.12}$	$1.54^{+0.25}_{-0.26}$
χ^2/dof	24/24	21/24	13/24	26/24	17/24	15/24
Fixed disk temperature						
T^{b}_{max}	1.9	2.0	2.0	2.1	2.1	2.4
N^{c}_{disk}	$11.8^{+3.4}_{-2.5}$	$12.0^{+3.0}_{-2.2}$	$13.4^{+3.4}_{-2.6}$	$9.2^{+1.6}_{-1.3}$	$5.5^{+1.2}_{-1.2}$	$2.7^{+0.9}_{-0.9}$
N^{d}_{gauss}	$4.4^{+1.2}_{-1.1}$	$4.8^{+1.3}_{-1.3}$	$3.9^{+1.4}_{-1.0}$	$3.9^{+1.2}_{-1.2}$	$4.4^{+1.2}_{-1.2}$	$4.6^{+1.4}_{-1.4}$
Γ^{e}	$1.5^{+0.2}_{-0.7}$	$1.6^{+0.2}_{-0.5}$	$1.5^{+0.3}_{-0.8}$	$1.7^{+0.1}_{-0.2}$	$1.9^{+0.1}_{-0.1}$	$2.1^{+0.1}_{-0.1}$
N^{e}_{powlaw}	$2.0^{+1.9}_{-1.6}$	$2.5^{+1.9}_{-1.8}$	$1.9^{+2.1}_{-1.7}$	$3.1^{+1.5}_{-1.5}$	$5.1^{+1.6}_{-1.5}$	$7.6^{+1.7}_{-1.7}$
F^{f}_{X}	$2.67^{+0.06}_{-0.14}$	$3.16^{+0.06}_{-0.20}$	$3.10^{+0.12}_{-0.48}$	$3.17^{+0.04}_{-0.09}$	$2.53^{+0.03}_{-0.02}$	$2.35^{+0.03}_{-0.02}$
F^{f}_{Disk}	$1.39^{+0.30}_{-0.15}$	$1.70^{+0.20}_{-0.19}$	$1.87^{+0.14}_{-0.18}$	$1.70^{+0.11}_{-0.21}$	$0.98^{+0.15}_{-0.16}$	$0.84^{+0.17}_{-0.25}$
F^{f}_{Power}	$1.20^{+0.12}_{-0.38}$	$1.43^{+0.15}_{-0.32}$	$1.27^{+0.14}_{-0.29}$	$1.51^{+0.10}_{-0.20}$	$1.48^{+0.16}_{-0.19}$	$1.49^{+0.12}_{-0.19}$
χ^2/dof	23/24	20/24	12/24	26/24	17/24	15/24

[a]We obtained six phase-averaged energy spectra where each spectrum is an average of all data within $1/6^{th}$ of the phase bin. [b]Accretion disk temperature in keV. We used the *diskpn* model in *XSPEC*. The inner radius of the disk was fixed at $6GM/c^2$. [c]Normalization of the *diskpn* component in units of 10^{-7}. [d]Normalization of the *gaussian* component (Fe Kα emission line) in units of 10^{-5}. The centroid energy and the width of the gaussian component were fixed at 6.55 keV and 0.33 keV as found by Caballero-García (2011). [e]Index (Γ) and the normalization ($\times 10^{-3}$) of the power-law component of the energy spectrum. [f]Total X-ray flux (F_X), Disk flux (F_{Disk}) and the power-law flux (F_{Power}) of the energy spectrum in the energy range of 3-15 keV (units are 10^{-11} ergs s^{-1} cm^{-2}. The column density of hydrogen along the line of sight was fixed at $1.1\times10^{22}cm^{-2}$ – the best-fitting value found by Feng & Kaaret (2010) using the high spatial resolution *Chandra* data.